SLAC-PUB-16491

Characterizing and optimizing photocathode laser distributions for ultra-low emittance electron beam operations*

F. Zhou,** D. Bohler, Y. Ding, S. Gilevich, Z. Huang, H. Loos, D. Ratner, and S. Vetter

SLAC, 2575 Sand Hill Road, Menlo Park, CA 94025, USA

ABSTRACT

Photocathode RF guns have been widely used for generating high-brightness electron beams for many different applications. The drive laser distributions in such RF guns play important roles in minimizing the electron beam emittance. Characterizing the laser distributions with measurable parameters and optimizing beam emittance versus the laser distribution parameters in both spatial and temporal directions are highly desired for high-brightness electron beam operation. In this paper, we report systematic measurements and simulations of emittance dependence on the measurable parameters for spatial and temporal laser distributions at the photocathode RF gun system of Linac Coherent Light Source. The tolerable parameter ranges for photocathode drive laser distributions in both directions are presented for ultra-low emittance beam operations.

Keywords: photoinjector; emittance; laser

1. Introduction

The performance of x-ray free electron lasers (FELs) [1-6] depends critically on the emittance of the electron beam. The electron beam is typically generated from an RF gun, and further accelerated to high energy with one or more stages of longitudinal bunch compression. The final projected and time-sliced beam emittances at the undulator, can be impacted by collective effects through acceleration and bunch compression, but they are dominated by the initial emittance from the RF gun. There are thermionic RF guns adopted in FEL [2], but the most popular RF guns [1,3-6] are based on the laser driven photocathode, from which the generated electron bunch could have lower emittance, lower energy spread, and flexibility of bunch length control. For example, at the Linac Coherent Light Source (LCLS), a typical electron bunch from the photo-injector would have a normalized emittance of about 0.4 μm (all emittance terms presented in this paper are normalized emittance), a rms sliced energy spread of ~1 keV, and a rms bunch length of 0.5 mm for 180-250 pC.

Optimizing photo-injector for achieving low-emittance electron beam is an important topic. Photo-injector source emittance is mostly dominated by photocathode thermal emittance, space-charge force induced emittance, and transverse radio frequency (RF) kick induced emittance [7]. The space-charge effect is sensitive to the photocathode drive laser parameters. Extensive studies have been performed in the past decades to mitigate the space charge effect for ultra-low emittance [8-14]. While the linear space-charge forces can be compensated by well-known solenoid focusing [12], the nonlinear space-charge forces (e.g. from non-uniform quantum efficiency distribution [11]) are more complicated. With the laser-driven photo-injector, one can manipulate the laser distribution to minimize the nonlinear space charge forces. For example, an ellipsoidal electron distribution would only have linear space-charge force which in principle can be completely compensated [15-16]. However, generation of an ellipsoidal laser pulse can be challenging. The existing techniques involving digital micro-mirror or spatial light modulator have problems caused by high losses and low damage threshold of optical components [17]. Studies also show that the emittance can be

This material is based upon work supported by the U.S. Department of Energy, Office of Science, Office of Basic Energy Sciences, under Contract No. DE-AC02-76SF00515.

improved with a simple laser distribution, the spatial truncated-Gaussian [18-19], which has been successfully implemented for the LCLS operation [18].

As discussed above, the electron beam quality can be optimized with manipulation of the drive laser. However, it is not always trivial to maintain a constant desired laser distribution for 24/7 operating laser systems. For example, the laser distributions are susceptible to external environment changes such as humidity and temperature, and also laser-related maintenance work. Thus, it is highly desirable to characterize photocathode laser shape with measurable parameters, and study the laser parameter tolerances for ultra-low emittance, which can guide the laser physicists to recover laser distributions within the desired ranges after laser work. This study performed at the LCLS injector can be directly adapted to other similar X-FEL facilities, such as Pohang X-FEL [4] and Swiss X-FEL [3] and European XFEL [6].

In this paper, we report electron beam emittance dependence on the laser spatial and temporal distributions based on simulations and measurements at the LCLS injector. A truncated-Gaussian spatial laser distribution is being used for this study and detailed characterization and optimization are discussed. This paper is organized as follows. Section II will introduce the measurements of the laser spatial distribution and emittance dependence on the parameters for drive laser spatial distributions. In Section III the emittance dependence on the temporal laser distribution (laser parameters) is presented. The tolerable laser parameter ranges for ultra-low emittance are summarized in Section IV.

2. Measuring and optimizing the spatial laser distribution

At the LCLS, the drive laser system is a frequency tripled, chirped-pulse amplification system based on a Ti:sapphire laser. The system consists of mode-locked oscillator, followed by a pulse stretcher, a regenerative amplifier, multi-pass amplifier, pulse compressor, and finally a frequency tripler to convert the IR laser to 253-nm ultraviolet beam. The 253-nm laser beam is finally delivered to the copper photocathode through a long in-vacuum transport from the laser room on the ground to the 10-m deep SLAC linac tunnel.

Many previous studies suggested that a photocathode drive laser with a uniform spatial distribution produces a lower emittance beam [20-21]. However, recent simulations and experimental observations at the LCLS show that the truncated-Gaussian spatial laser profile produces a better emittance beam than a uniform one does. This is because the space charge in the truncated-Gaussian case is more linear, resulting in better emittance compensation [18]. Figure 1 (top) shows the simulated different spatial lineout distributions (intensity projection to x (y) plane for the central transverse-slice beam in y (x) plane) including pseudo-uniform (a), truncated-Gaussian (b), and Gaussian-like (c). The ratio g/h shown in Fig. 1 (top, b) determines the laser shape. The projected and time-sliced emittances of three distributions are simulated, as shown in Fig. 1 (bottom), using ImpactT code [22] for 150 pC. In all simulations, 0.9 μm/mm of the measured thermal emittance is included. The emittance with the spatial truncated-Gaussian distribution improves 15-25% in comparison to the pseudo uniform laser or Gaussian-like one. For a uniform profile, an emittance bump for the core slices is observed. This is probably due to the strong space charge effects.

The following subsections present two methods of laser spatial shape characterization: spatial laser lineout distribution and Zernike modes [23]. These subsections present, both measurable laser beam parameters and associated tolerances for an ultra-low emittance beam.

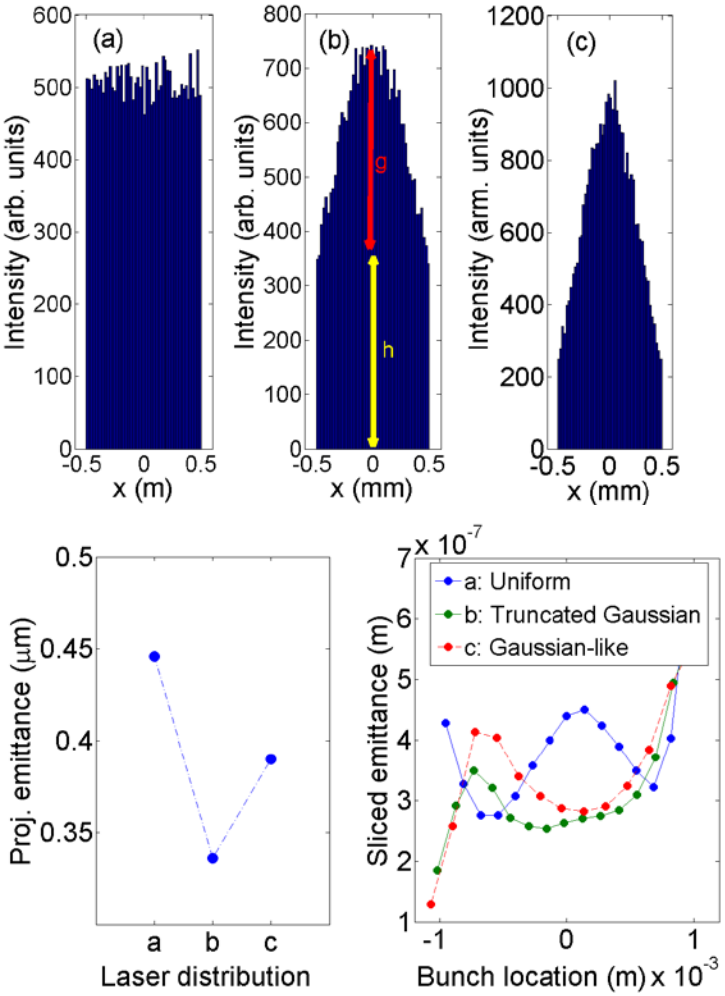

Fig.1. Simulated spatial laser lineout distributions (top): (a), (b) and (c) represent pseudo uniform, certain truncated-Gaussian and Gaussian-like spatial distributions; corresponding simulated projected (bottom, left) and slice emittances (bottom, right) for 150 pC.

2.1 Parameterized with laser lineout distribution and emittance dependence on the laser parameters

When the laser on the photocathode has a reasonably clean spatial profile (shown in Fig. 2 as an example), a simple way to quantify laser distribution is to use the lineout-distribution method. The lineout intensity ratio g/h is used to determine the laser beam spatial shape. The spatial laser distribution is pseudo uniform with g/h<0.1, while with g/h>3 it is near Gaussian. Figure 3 shows both simulated and measured projected emittances for different g/h with 150 pC electron beam charge. Both measurements and simulations show that the optimum emittance is obtained with g/h ~1. The results indicate that emittance growth can be maintained <5% with g/h in about 1±0.25. The simulated emittance is smaller than the measured one because in the simulations a perfectly smooth laser profile has been used. The difference between measured and simulated emittances does not impact the conclusion for the tolerated g/h range for the ultra-small emittance. For a reasonably smooth spatial Gaussian laser beam, g/h can be easily adjusted within the desired range by adjusting an optical zoom telescope placed before the iris (aperture) that is relay imaged to the photocathode. Note that all projected emittance measurements [24] reported in this paper use a wire scanner located at 135-MeV injector. A Gaussian fit was used for calculation of the beam size after subtraction of the background for the wire scanner measurements.

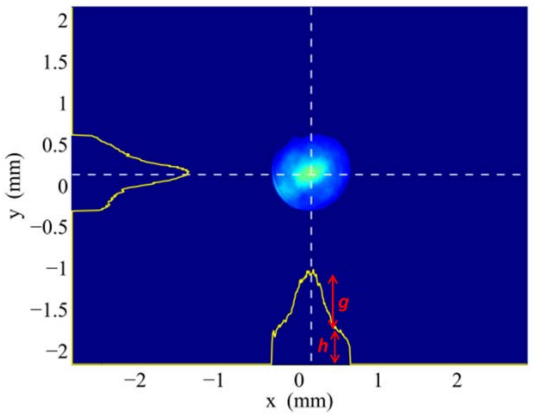

Fig.2. Example of a reasonably smooth photocathode laser distribution parameterized by the lineout intensity ratio *g/h*.

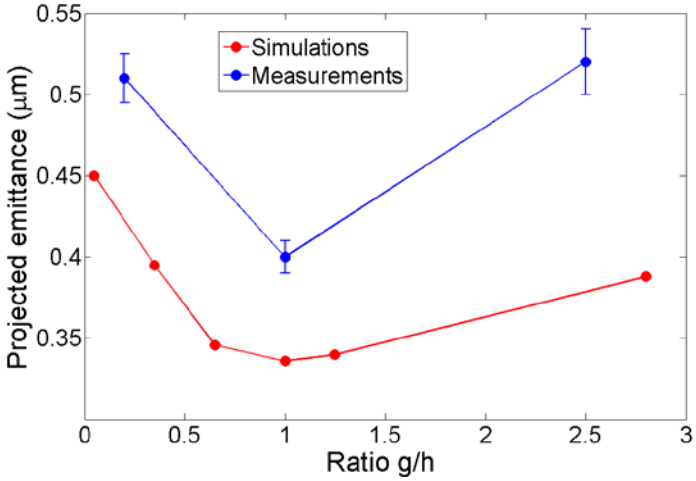

Fig.3. Simulated and measured projected emittance for different g/h of lineout intensity ratio for 150 pC.

The simulations also indicate that the optimum emittance can be obtained with hard edge height $a_1=a_2$ shown in Fig. 4 (top). However, during routine operations, a_1 and a_2 are hard to keep balanced. So what is the tolerated range of a_1/a_2 for ultra-low emittance? Simulations show that with the ratio a_1/a_2~1±0.3 the projected emittance growth can be controlled <5%.

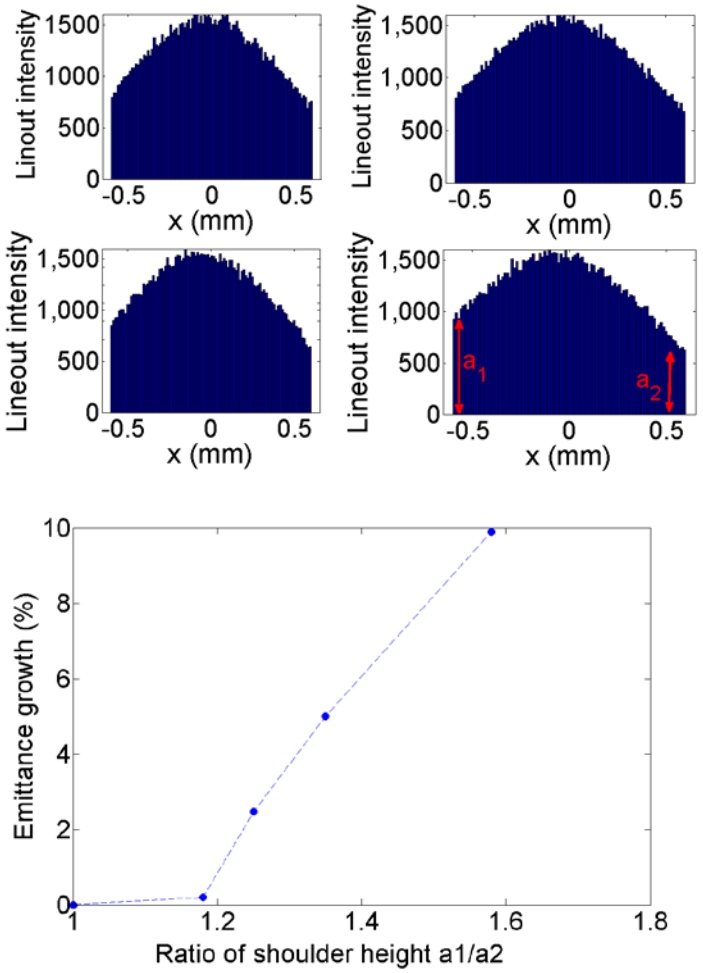

Fig. 4. Line-out distribution with different ratio of laser hard edge heights a_1/a_2 (top), and simulated projected emittance growth as function of a_1/a_2 (bottom) for 150 pC.

2.2 Parameterized with laser Zernike modes and emittance dependence on the parameters

In practice, it is hard to make the ultraviolet spatial laser distribution on the cathode be smooth. In such case, using lineout distribution parameters may not fully represent a true laser beam. The parameters for laser Zernike modes are found to better characterize the spatial laser distributions, although they require additional calculation.

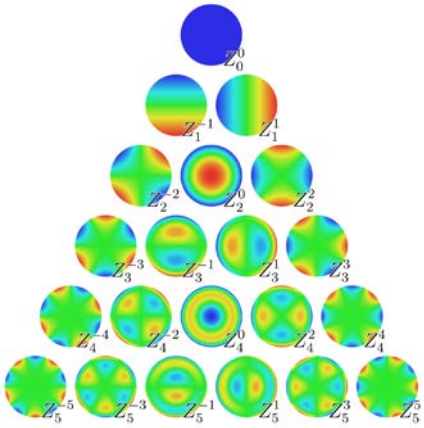

Fig. 5. Example of twenty-one Zernike modes Z_n^m.

Zernike functions are widely used in optical systems to characterize the measured structures of deformations and aberrations, because they are orthogonal over the unit circle. Figure 5 shows the first twenty-one Zernike modes Z_n^m [23]. The Zernike functions are a product of the Zernike radial polynomials and sine- and cosine-functions [25]:

$$\begin{Bmatrix} Z_n^m(r,\theta) \\ Z_n^{-m}(r,\theta) \end{Bmatrix} = R_n^m(r) \begin{Bmatrix} \sin m\theta \\ \cos m\theta \end{Bmatrix} \qquad (1)$$

Where index n is positive integer, i.e., n=0, 1, 2 …; m is positive integer, i.e., 0≤m≤n with (n-m) even; θ is the azimuthal angle with 0≤θ≤2π, r is the radial distance with 0≤r≤1. Radial polynomial R(r) is usually defined as function of r:

$$R_n^m(r) = \sum_{k=0}^{(n-m)/2} \frac{(-1)^k (n-k)!}{k!\left(\frac{n+m}{2}-k\right)!\left(\frac{n-m}{2}-k\right)!} r^{n-2k} \qquad \text{n=0, 1, 2 …; 0≤m≤n with (n-m) even} \qquad (2)$$

As Zernike functions are orthogonal over the unit circle, they satisfy the following condition [25]:

$$\iint Z_n^m Z_{n'}^{m'} r dr d\theta = \frac{1}{2n+1} \delta_{nn'} \delta_{mm'} \qquad (3)$$

Thus, any complex function *f(r,θ)* (such as laser shape) defined on the circle can be expressed as a sum of Zernike modes:

$$f(r,\theta) = \sum_{n=0}^{\infty} \sum_{m=-n}^{n} a_{nm} Z_n^m(r,\theta) \qquad (4)$$

Then the coefficients a_{nm} for Zernike modes in Eq. 4 are given by:

$$a_{nm} = \iint f(r,\theta) Z_n^m(r,\theta) r dr d\theta \qquad (5)$$

At the LCLS, the Zernike mode coefficients a_{nm} are calculated for the injector drive laser images on the photocathode. The coefficients a_{nm} are represented for contribution of each mode to the spatial laser image. For simplicity, two parameters, so called symmetry and asymmetry powers, representing all mode coefficients are used to quantify actual laser distribution. Namely, the symmetry power, $p_{symmetry}$, is calculated by summing the squares of the coefficients for m=0 modes (except the first m=0 mode) normalized by the square of the coefficient for the first m=0 mode, i.e., $\sum_n {a_{n0}}^2 / {a_{00}}^2$, where n≠0;. As shown in Fig. 5, $p_{symmetry}$ for modes with m=0 determines the laser shape, whether it is Gaussian, truncated-Gaussian or uniform. The asymmetry power, $p_{asymmetry}$, is estimated by summing the squares of the remaining mode coefficients normalized by the square of the coefficient for the first m=0 mode, i.e., $\sum_{n,m} {a_{nm}}^2 / {a_{00}}^2$, where m≠0. $p_{asymmetry}$ determines the degree of the laser beam profile symmetry in x and y planes. In the LCLS experiment, the first forty five modes were required to reconstruct beam image with reasonably high resolution. Pseudo-uniform and pure Gaussian laser distributions correspond to $p_{symmetry}$<1% and >7%, respectively. When the laser profile is reasonably symmetric in both x and y planes, the $p_{asymmetry}$ is <1%.

Figure 6 shows three different laser images illuminating the LCLS cathode (d is the pseudo uniform laser, e and f are truncated-Gaussian laser beams with different degrees of truncations) and the projected emittance dependence on their relevant $p_{symmetry}$ (bottom) for 150 pC, with a fixed $p_{asymmetry}$<1%. The experimental data shows that the ultra-small emittance can be maintained with the $p_{symmetry}$ within 2.5-4% (truncated Gaussian distributions). With the lineout method, the g/h value for images e and f shown in Fig. 6 (top) is in between 0.75-1, within the tolerated range for good emittance. So, both methods are consistent in term of emittance. Figure 7 shows the measured projected emittance

dependence on the laser beam asymmetry power, for a fixed $p_{symmetry}$= 2.5%. The measurement shows that the projected emittance growth can be controlled <5% with the $p_{asymmetry}$<1.5%.

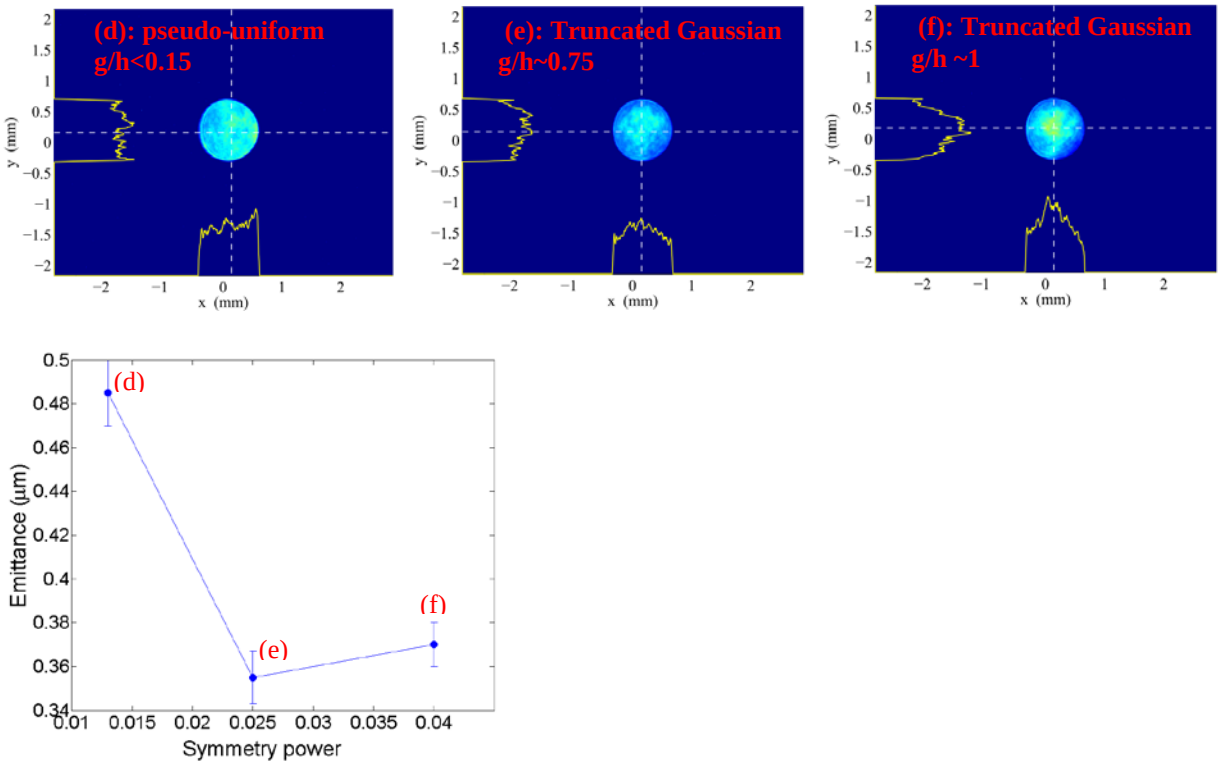

Fig.6. Photocathode laser shapes; measured projected emittance vs. symmetry power relevant to three laser shapes with fixed asymmetry $p_{asymmetry}$<1%.

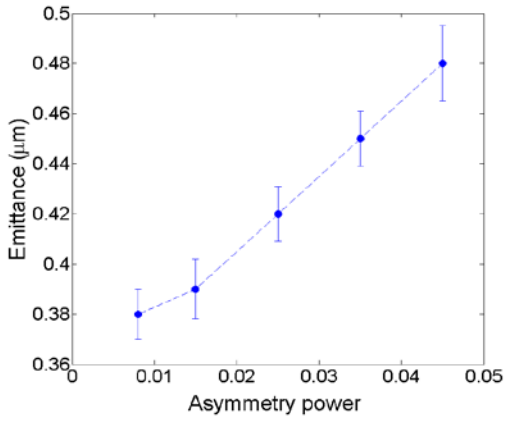

Fig.7. Measured emittance dependence on the asymmetry power for a fixed $p_{symmetry}$= 2.5%.

3. Optimizations of temporal laser distribution

RF kick induced emittance ε_{rf} and space charge emittance ε_{sc} strongly depend on the photocathode drive laser pulse length [7], expressed by:

$$\varepsilon_{rf} \sim E \cdot \sigma_r^{\,2} \cdot \sigma_z^{\,2} \qquad (6)$$

$$\varepsilon_{sc} \sim \frac{Q}{E \cdot \sigma_z} \mu_x \qquad (7)$$

where E is the peak accelerating gradient on cathode, μ_x is the transverse space charge factors related to the aspect ratio of the rms beam size σ_r to rms bunch length σ_z, and Q is the bunch charge. Eqs. 6 and 7 indicate that the laser pulse length has to be traded off between space charge force and RF kick emittance for an optimum emittance. Systematic simulations of the emittance dependence on the single Gaussian temporal laser length are performed for 180 pC and shown in Fig. 8. The simulations show that the projected (left) and sliced emittances (right) are nearly optimal with a single ~3.5 ps FWHM Gaussian laser.

The current LCLS drive laser pulse is 2.0±0.2 ps FWHM in length. For the LCLS drive laser systems, it is difficult to lengthen laser pulse length >3 ps FWHM without compromising the temporal laser shape. Lengthening the laser pulse requires the lasers to operate under- or over-compression with the introduction of a chirp. The chirp may cause the deformation of temporal laser profile. Instead, two ~2 ps s- and p-polarization Gaussian laser pulses are stacked together with a certain separation to lengthen the laser pulse. The advantages of using pulse stacking over a single long Gaussian laser pulse are: 1) flexibility to adjust overall laser pulse length for various needs; 2) relatively sharper edges (i.e., faster rise/fall time) of the laser pulse for better emittance compensation process. Simulations shown in Fig. 8 confirmed that a better projected emittance is expected with a stacked ~4 ps FWHM pulse (~2 ps separation for stacking two 2-ps pulses) than a single 3.5 ps FWHM Gaussian laser pulse.

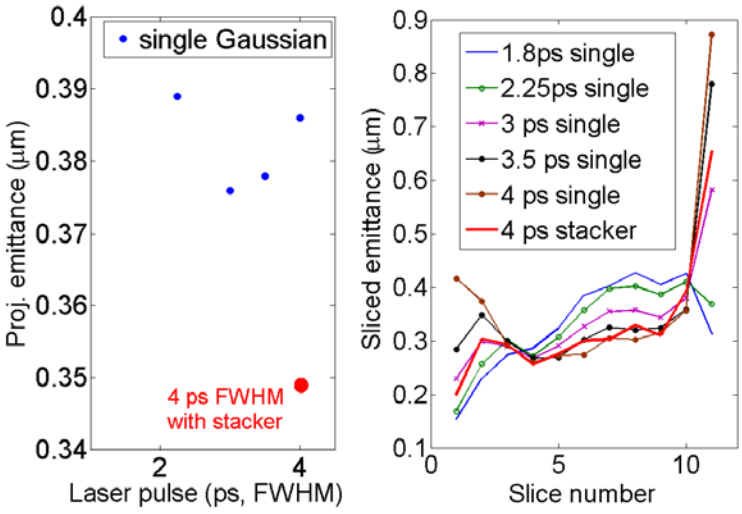

Fig.8. Simulated projected (left) and sliced (right) emittance dependence on a single Gaussian laser and a stacked pulse 4 ps FWHM for 180 pC.

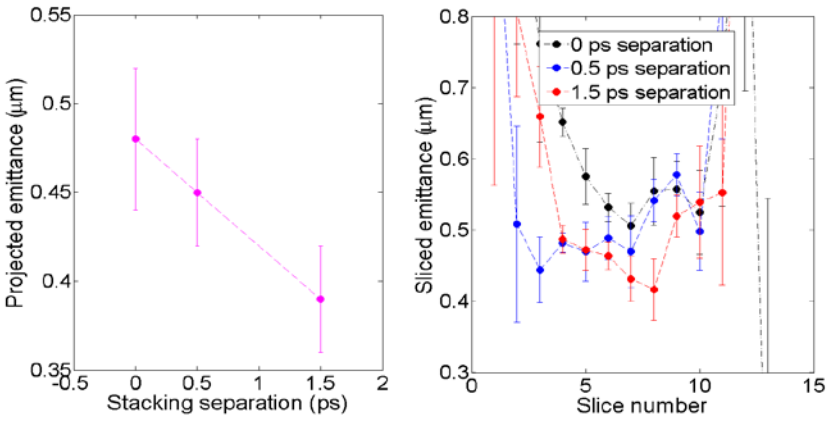

Fig.9. Measured projected (left) and slice (right) emittance (250 pC) with different pulse separation for stacking two ~2 ps FWHM pulses.

Figure 9 shows the comparison of the measured projected (left) and sliced (right) emittances for a single ~2 ps Gaussian and stacked two 2-ps laser pulses with different separations. The measured projected emittance is significantly improved with 1.5 ps separation of the pulse stacking compared with a single 2 ps Gaussian (i.e., overlapping the s-polarized with p-polarized pulse). Simulations and measurements show that the emittance can be slightly further improved with the pulse separation up to 2 ps. But we chose 1.5-ps separation for LCLS operations to avoid some parasitic effects in the longitudinal dimension due to a longer initial bunch and the possibility of an intensity dip with larger separation for pulse stacking. The slice emittance shown in Fig. 9 (right) is measured with an S-band transverse deflector and an optical transition radiation (OTR) screen at 135-MeV injector with the laser heater chicane turned-off to avoid coherent OTR on the screen [24]. An rms 5% area cutting is used for beam size measurements from the OTR measurements after subtraction of the background. The details of emittance measurements are described in Refs. [18, 24]. The measured slice emittance is significantly improved with 1.5 ps separation for the pulse stacking, in comparison to single Gaussian 2-ps laser for 250 pC. During the emittance measurements shown in Fig. 9 (right), the spatial laser profile on the cathode is not necessarily optimized for optimal emittance but is kept unchanged for fair comparisons. The x-ray FEL pulse intensity is eventually improved by 30-50% with the stacked laser pulse compared with a single Gaussian ~2 ps FWHM laser pulse. This is consistent with emittance improvement with the stacked laser pulse.

4. Summary

Characterizing and controlling transverse laser distribution on the photocathode with measurable parameters is highly desired for maintaining an ultra-low emittance beam at the LCLS. Quantitative measurements of the laser pulse spatial distribution parameters using lineout distribution and Zernike polynomials are developed. According to measurements and simulations, projected emittance growth can be controlled <5% with spatial laser parameter g/h of 1±0.25 and ratio of laser hard edge heights a1/a2 of 1±0.3, using a lineout distribution method, or of symmetry power in between 2.5-4% and asymmetry power <1.5% using the Zernike modes method. Measurements and simulations also indicate that ultra-small emittance can be achieved with the stacked 3.5-4 ps (1.5-2 ps separation for stacking two single 2 ps FWHM pulses) FWHM for 180-250 pC.

These quantified criteria for spatial and temporal laser pulse shape distributions can guide laser scientists to recover laser pulse shape within the desired ranges in order to achieve high-brightness x-ray FEL operation. These results are not only useful for LCLS injector but also for similar X-FEL injectors such as SWISS X-FEL and Pohang X-FEL injectors and the described methods are of general importance for photoinjectors required to stably generate high brightness electron beams.

* The work is supported by DOE under grant No. DE-AC02-76SF00515.
** zhoufeng@slac.stanford.edu

References

[1] P. Emma *et al*., „first lasing and operation of an Angstrom-wavelnegth free electron laser“, Nature Photon. 4 641 (2010).

[2] T. Ishikawa *et al*., „A compact x-ray free electron laser emitting in the sub-angstrom region“, Nature Photonics 6, 540-544 (2012).

[3] H. H. Braun, „SWISSFEL, the X-ray Free Electron Laser at PSI“, Proceedings of FEL2012, Nara, Japan.

[4] H.-S. Kang, K.W.Kim, I.S.Ko, „Status of the PAL XFEL construction“, Proceedings of IPAC2015, Richmond, VA, USA.

[5] W. Ackermann et al., „Operation of a free-electron laser from the extreme ultraviolet to the water window“, Nature Photonics 1, 336-342 (2007). http://www.nature.com/nphoton/journal/v1/n6/abs/nphoton.2007.76.html

[6] W. Decking, F. Le Pimpec, „European XFEL construction status“, Proceedings of FEL2014, Basel, Switzerland. http://accelconf.web.cern.ch/AccelConf/FEL2014/papers/web03.pdf

[7] K-J. Kim, Nucl. Instrum. Methods Phys. Res. Sect. A 275, 201 (1989).

[8] R. Akre et al., “Commissioning the linac coherent light source injector”, Phys. Rev. ST-AB 11, 030303 (2008).

[9] M. Krasilnikov et al., „Experimentally minizied beam emittance from an L-band photoinjector“, Phys. Rev. ST-AB 15, 100701 (2012).

[10] E. Prat et al., „Emittance measurements and minimization at the SwissFEL injector test facility“, Phys. Rev. ST-AB 17, 104401 (2014)

[11] F. Zhou, I. Ben-Zvi, M. Babzien, X. Chang *et al*., “Experimental characterization of emittance growth induced by the nonuniform transverse laser distribution in a photoinjector”, Phys. Rev. ST-AB 5, 094203 (2002).

[12] B. Carlsten, “New photoelectric injector design for the LOS Alamos National Laboratory XUV FEL Accelerator”, Nucl. Instr. Methods A285, 313 (1989).

[13] J. Gallardo and R. Palmer, “emittance correction of photocathode gun”, Nucl. Instr. Methods A304 (1991) 345-347.

[14] M. Ferarrio et al., “Conceptual design of the TESLA XFEL photoinjector”, TESLA-FEL 2001-03 http://flash.desy.de/sites2009/site_vuvfel/content/e403/e1642/e772/e77

[15] P. Piot *et al*., “Formation and acceleration of uniformly filled ellipsoidal electron bunches obtained via space charge driven expansion from a cesium-telluride photocathode”, Phys. Rev. ST Accel. Beams 16, 010102 (2013).

[16] M. Bakr, M. Khojoyan, M. Krasilnikov, F. Stephan, G. Vaschenko, “Beam dynamics simulation for the upgraded PITZ photocathode laser pulse shapes”, Daejeon, South Korea, FEL15

[17] S. Li et al., “LCLS injector laser modulation to improve FEL operation efficiency and performance”, Proceedings of IPAC2015, Richmond, VA. http://accelconf.web.cern.ch/AccelConf/IPAC2015/papers/tupje074.pdf

[18] F. Zhou, A. Brachmann, P. Emma, S. Gilevich, and Z. Huang, “Impact of the spatial laser distribution on photocathode gun operation”, Phys. Rev. ST-AB 15, 090701 (2012).

[19] M. Hanel, “Experimental investigations on the influence of the phtocathode laser pulse parameters on the electron bunch quality in an RF-photoelectron source”, Ph. D thesis at Hamburg University, 2010.
http://www-library.desy.de/preparch/desy/thesis/desy-thesis-10-027.pdf

[20] SwissFEL conceptual design report, July 2010.
https://www.psi.ch/swissfel/HomeEN/SwissFEL_CDR_web_small.pdf

[21] LCLS FEL conceptual design report, SLAC-R.593, April 2002. http://www-ssrl.slac.stanford.edu/lcls/cdr/lcls_cdr-ch06.pdf

[22] J. Qiang, ImpactT code manual, LBNL-62326, 2007.

[23] Zernike function see link below: https://en.wikipedia.org/wiki/Zernike_polynomials

[24] F. Zhou, K. Bane, Y. Ding, Z. Huang, H. Loos, and T. Raubenhemier, “Measuring and analysis of a high-brightness electron beam collimated in a magnetic bunch compressor”, Phys. Re. ST-AB 18, 050702 (2015).

[25] P. Fricker, analysing lasik optical data using Zernike functions, http://www.mathworks.com/company/newsletters/articles/analyzing-lasik-optical-data-using-zernike-functions.html